Conformational Properties of Nickel(II) *meso*-Tetraphenylporphyrin in Solution. Raman Dispersion Spectroscopy Reveals the Symmetry of Distortions for a Nonplanar Conformer

Esko Unger, Wolfgang Dreybrodt, and Reinhard Schweitzer-Stenner*

Institut für Experimentelle Physik, Universität Bremen, P.O. Box 330440, 28334 Bremen, Germany

Received: February 18, 1997; In Final Form: June 17, 1997[⊗]

We have measured the Raman spectra of nickel(II) tetraphenylporphyrin (NiTPP) in CS_2 with excitation wavelengths covering the region of the Q_0, Q_ν, B_0, and B_ν absorption bands. The spectra were subjected to a global fit which provides reliable spectral parameters even in the case of strongly overlapping bands. The band shapes of ν_8, Φ_8, ν_1, ν_{11}, ν_{19}, ν_2, and ν_{10} are clearly asymmetric and can be decomposed into two sub-bands, the intensity ratios of which depend on the excitation wavelength. The Raman excitation profiles (REPs) of the low-frequency sub-bands of the core size marker bands ν_{11}, ν_{19}, ν_2, and ν_{10} are red shifted with respect to the REPs of the corresponding high-frequency sub-bands. The REPs of the ν_8 sub-bands also show different resonance positions, but in this case the REP of the high-frequency sub-band is the red-shifted one. The sub-bands exhibiting the red-shifted REPs result from a nonplanar conformer, whereas the other sub-bands correspond to a planar form. On the contrary, the REPs of the ν_1 and Φ_8 sub-bands can be scaled onto each other. Their heterogeneity results either from Fermi resonance or from additional conformations of the NiTPP molecules which may differ in the orientation of their phenyl substituents. Information about the modes of distortion giving rise to the nonplanar structure are obtained from the wavelength dependence of the depolarization ratios. The depolarized B_{1g} and B_{2g} bands show no dispersion. On the contrary, some A_{1g} bands show a slight and a few A_{2g} bands even a strong DPR dispersion resulting from of an electronic A_{2g}-type perturbation. This indicates that the nonplanar conformer exhibits two types of symmetry-lowering distortions, namely, ruffling (B_{1u}) and saddling (B_{2u}). This parallels recent findings on NiTPP crystals. Thus evidence is provided that the nonplanar species of NiTPP in solution is structurally similar to the conformation observed in the crystallized phase.

1. Introduction

Metalloporphyrins are organic compounds that play a major role in the metabolism of plants and animals. In the absence of external forces and steric crowding of the porphyrin substituents the macrocycle exhibits D_{4h} symmetry. This is because the energy of the π electronic system is lowest for a planar conformation. In this high symmetry, the depolarization ratio (DPR) of the A_{1g}, A_{2g}, B_{1g}, and B_{2g} Raman-active fundamentals is independent of the exciting laser frequency. A_{1g} modes exhibit a value of 1/8, B_{1g} and B_{2g} modes a value of 3/4, and A_{2g} modes a value of infinity. Experimental results on biological systems, however, where the porphyrin is embedded in a protein matrix of low symmetry, have shown that the depolarization ratios are strongly dispersive.[1−4] The dispersion is caused by out-of-plane and to a minor extent by in-plane distortions of the porphyrin macrocycle, which can both be classified in terms of the irreducible representations of the D_{4h} symmetry group. Jentzen et al.[5] have investigated the X-ray structures of prosthetic groups in several heme proteins. They found that the predominant nonplanar distortions are ruffling, saddling, and doming, corresponding to the representations B_{1u}, B_{2u}, and A_{2u}. The symmetry type and magnitude of these distortions differ for various heme groups in proteins, even for different subunits of human deoxyhemoglobin. In the α subunit, the heme group is ruffled and domed, whereas saddling and doming are the main distortions in the β chain.[5]

There is evidence that such macrocycle distortions can modulate the efficiency of the heme group's biochemical function, e.g., the electron transfer in the photoreaction centers[6,7] and in various cytochrome derivatives[5] as well as the enzymatic activity of methylreductase.[8] Moreover, investigations of the structure−function relation of a series of porphyrins with varying degree of nonplanarity[7,9] suggest that nonplanar distortions hinder axial ligation and reduce the oxidation potential of the macrocycle. These results indicate that the protein controls the heme group's function by transferring changes of the tertiary structure to its interface with the heme group to induce specific asymmetric distortions of the macrocycle. This affects functions like oxygen binding or electron transport.[3,4]

In order to explore the intrinsic parameters that determine the conformation of the macrocycle, a variety of synthetic metalloporphyrins with different substituents and central metal ions were investigated.[9−14] Comparison of the UV−vis and the Raman spectra of these porphyrins has shown that some Raman lines as well as the Q and B absorption bands are sensitive to changes of the porphyrin conformation. The frequency positions of these structure-sensitive bands were then correlated with specific structural parameters obtained from molecular mechanics calculations and crystallographic data. The magnitude of out-of-plane distortions was found to increase with decreasing core size and with increasing bulkiness of the peripheral substituents.

In crystals, the packing forces have a strong impact on the porphyrin structure. X-ray investigations of the three crystal forms of nickel octaethylporphyrin (NiOEP) show that the porphyrin is planar in the triclinic A and B forms, but ruffled in the tetragonal crystal,[15] while planar and nonplanar conformations coexist in noncoordinative solution.[16,17] However, the differences between the frequency positions of the structure-sensitive Raman bands in the spectra of crystallized and

* Author to whom all correspondence should be addressed. FAX: +49-421-218-7318. E-mail: stenner@theo.physik.uni-bremen.de, unger@theo.physik.uni-bremen.de.

[⊗] Abstract published in *Advance ACS Abstracts,* August 1, 1997.

S1089-5639(97)00606-3 CCC: $14.00

dissolved NiOEP indicate that the nonplanar structure in solution must be different from the conformation in the tetragonal crystalline form. Additionally, the Raman spectra in the low-frequency region, in which most of the lines arising from out-of-plane vibrational modes are expected, are quite different for NiOEP in solution and in the tetragonal crystal. Because enhancement of these lines, which are Raman-inactive in D_{4h} symmetry, depends on the type and strength of nonplanar distortion, the Raman data suggest that these distortions in solution might be different from those in the crystal, and it is even conceivable that other modes of distortions are predominantly operative.

The present work is aimed at further exploring the structure of the conformers of *meso*-substituted nickel(II) tetraphenylporphyrin (NiTPP) in solution. Recent Raman experiments have provided evidence[18] that this porphyrin parallels NiOEP in that planar and nonplanar conformations coexist in CS_2. Contrary to NiOEP, only one crystal form is known,[18] in which the porphyrin exhibits a nonplanar conformation that is predominantly ruffled with a significant contribution from saddling. The question arises whether these distortions are also present in the nonplanar conformation in solution.

Information about symmetry lowering distortions can be obtained by analyzing the depolarization ratios (DPRs)[2,19] of Raman lines. If only one type of out-of-plane distortion of odd symmetry (e.g. ruffling: B_{1u}) is operative, the depolarization ratios of the Raman bands are the same as in D_{4h} symmetry.[20] The presence of two nonplanar distortions of different symmetry, however, can cause a DPR dispersion (DPD). Ruffling and saddling (B_{1u} and B_{2u}), for example, induce a perturbation of type $B_{1u} \times B_{2u} = A_{2g}$ that causes dispersion of the polarized and inverse polarized Raman lines, while the DPRs of the depolarized lines remain constant. We therefore investigate the DPDs of several fundamental lines in order to identify the out-of-plane distortions of the nonplanar conformer of NiTPP.

Additional information about the conformations of NiTPP can be extracted from the resonance excitation profiles (REPs) of the structure-sensitive Raman bands.[21] Jentzen et al.[18] have shown that two of these bands, i.e. ν_8 and ν_2, are composed of at least two sub-bands. The intensity ratios of corresponding sub-bands depend on temperature. Moreover, they are different at the two excitation wavelengths (413.1 and 457.9 nm) employed. The high-frequency (HF) sub-band of ν_8 and the low-frequency (LF) sub-band of ν_2 are more intense at 457.9 nm excitation. This was interpreted as a red shift of these sub-bands' REPs compared to those of the corresponding sub-bands. However, this conclusion is not compelling because the REPs may be different even if they are nonshifted. It has been shown[4,22] that in the preresonance region of the B_0 band the Raman intensity is determined by interferences between intrastate Franck−Condon and interstate Herzberg−Teller coupling. If the coupling parameters have different signs, the preresonance intensity is relatively high. This may be the case for the HF sub-band of ν_8. In order to find the correct explanation for the dispersion of the above intensity ratios, we have determined the REPs of the sub-bands of all structure-sensitive bands using excitation wavelengths that cover the entire region of the Q and B bands. By means of a sophisticated global analysis, where all spectra were consistently fitted using identical band shapes, half-widths, and frequencies for each sub-band, we were able to decompose these asymmetric bands and to obtain the REPs for each conformer.

2. Materials and Methods

Preparation. NiTPP was purchased from Porphyrin Products (Logan, Utah) and was further purified by liquid chromatography using CS_2 (Aldrich, HPLC grade) as the mobile phase (column 1 × 10 cm^2; Silica 32-63, 60 A, ICN Biomedicals). The homogeneity of the sample was checked by thin-layer chromatography using Kieselgel with fluorescence indicator F254 (Merck).

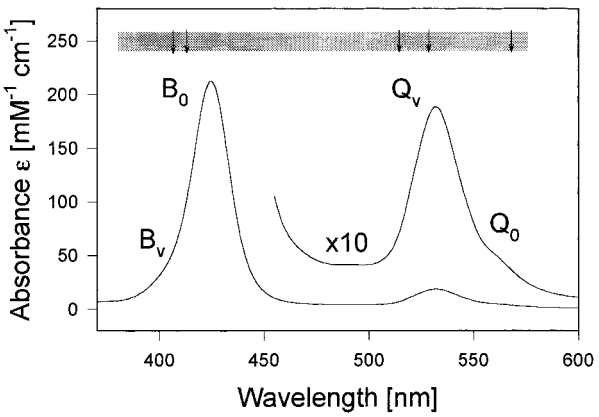

Figure 1. UV−vis spectrum of NiTPP in CS_2. The gray bar indicates the range of excitation wavelengths used for the Raman measurements with the excimer pumped dye laser. The arrows mark the wavelengths used for CW excitation.

UV−Vis Absorption. After drying the purified NiTPP in vacuum (at 60 °C for 2 h) 3.36 mg of the porphyrin was dissolved in 5 mL of CS_2 to yield a concentration of 1 mM. After further diluting the sample to 0.02 mM UV−vis spectra were taken with an diode array spectrometer (Hewlett-Packard 8451 A) using a cuvette with an optical pathway of 1 mm. Figure 1 depicts the absorption spectrum in units of mM^{-1} cm^{-1}. The band positions (and maximum extinction coefficients) are 425 nm (217 mM^{-1} cm^{-1}) for the B_0 band and 532 nm (18.9 mM^{-1} cm^{-1}) for the Q_ν band.

We have checked this method to determine the absolute extinction coefficients by applying the analogous procedure to NiOEP in CS_2, for which the absorbance is known.[17] Thus we obtained a maximum extinction of 155 mM^{-1} cm^{-1} for the B_0 band. The value previously obtained[17] is 170 mM^{-1} cm^{-1}, and we therefore estimate an error of about 10%.

Resonance Raman Spectroscopy. The resonance Raman spectra were recorded by using two Raman setups.

Excimer Pumped Dye Laser System. Raman spectra at a large number of different excitation wavelengths were obtained by utilizing an excimer (Lambda EMG53MSC) pumped dye laser (Lambda FL2001) system. All measurements were carried out in backscattering geometry. The spectra were recorded with excitation wavelengths between 380 and 576 nm with an average distance of 3 nm to cover the Q_0, Q_ν, B_0, and B_ν resonance region. The pulse energy was 1 mJ at a 200 Hz repetition rate and a pulse length of about 10 ns. Thus, an average power of 200 mW was provided. The scattered light was filtered by two pinholes and focused by a cylindrical lens of 50 cm focal length onto the sample placed in a cylindrical rotating quartz cell. Rotation of the Raman cell (50 Hz) prevented local heating of the absorbing sample. The scattered light was collected and imaged onto the entrance slit of the spectrometer. A polarization analyzer between collimator and entrance slit was used to measure the Raman intensity of the two components parallel ($\parallel$) and perpendicular ($\perp$) to the incident laser polarization. A polarization scrambler was placed in front of the entrance slit to avoid different transmissions of the spectrometer for the above polarization components.

The scattered light was dispersed by a Czerny-Turner monochromator (Spex 1877) equipped with a grating with 1200 grooves/mm. The geometrical slit S was adjusted either to 50

μm or to 100 μm. A preceding double monochromator was used as a filter to suppress stray light. The scattered light was detected by a CCD camera (Photometric series 200, 5700051 version 6.0) cooled with liquid nitrogen. The collected data were stored in a computer.

In order to obtain the true Raman band shapes, the observed bands were deconvoluted with the slit function of the spectrometer. These spectral slit functions were determined by recording the spectral lines of several pencil lamps (xenon, krypton, etc.). They are well approximated by Gaussians for 50 μm and by convolution of a Gaussian and a boxcar function for 100 μm slit width. The half-width of the spectral slit function increases for decreasing wavelengths. In order to get a sufficient resolution, we always used a slit width of 50 μm for excitation between 380 and 432 nm. The corresponding spectral width, defined by the full width at half-maximum (fwhm), is 6.9 cm^{-1} at 380 nm and 5.0 cm^{-1} at 430 nm excitation (for a Stokes shift of 1000 cm^{-1}). For excitation wavelengths higher than 432 nm we used a slit width of 100 μm in most cases, thus providing a spectral width of 8.4 cm^{-1} (boxcar 7.6, Gaussian 3.5) at 440 nm excitation, and 4.5 cm^{-1} (boxcar 4.0, Gaussian 2.0) at 570 nm. It has to be noted that the device-limited spectral resolution of the CCD array is about 1 cm^{-1}, which is smaller than all spectral widths used in our experiments.

The frequency calibration of the Raman spectra was carried out by using the intense 656 cm^{-1} line of the CS_2 solvent, which also served as an internal standard for determining the intensities of the porphyrin Raman bands. The dispersion of the spectrometer was earlier obtained using the spectra of the pencil lamps. The wavelength dependence of the dispersion was accounted for in the calibration procedure. The maximum error of the observed line positions at different excitation wavelengths is 1.5 cm^{-1}. The obtained REPs were corrected for the sample's absorption as described in a previous study.[22] We used a porphyrin concentration of about 0.5 mM for B band excitation and 1.0 mM otherwise.

CW Laser System. Supplementary measurements with higher spectral resolution were carried out with CW excitation provided by either an argon ion laser (Spectra-Physics, Model 2020-05) or a krypton ion laser (Coherent, Innova 90 K). The plasma light of these lasers was suppressed by using interference filters. The measurements were performed with backscattering geometry. By using a cylindrical lens of 10 cm focal length, the linear polarized laser beam was focused onto the sample placed in a 10 mm quartz cuvette (Starna). The scattered light was collected and imaged on the entrance slit of the spectrometer (Spex 1401) equipped with a CCD camera (Photometrics, SDS 9000) containing a 512 $\times$ 512 array chip (Site, TK 512 CB). The data were stored in a computer which also controls the motor of the spectrometer. Polarized Raman spectra were recorded by using a polarization filter as analyzer (Spindler & Hoyer) and a scrambler placed in front of the entrance slit of the spectrometer.

The spectral slit functions were again determined by the spectral lines of pencil lamps (krypton, argon, etc.) and can be described by convolution of a Gaussian and a boxcar function. The entrance slit was adjusted to $S = 100$ μm for excitation at 406.7 and 413.1 nm and to $S = 200$ μm for all other excitation wavelengths used. The spectral width is about 2.7 cm^{-1} (boxcar 2.3, Gaussian 1.4) at 406.7 and 413.1 nm excitation. For $S =$ 200 μm, this width is 2.8 cm^{-1} (boxcar 2.7, Gaussian 0.9) at 514.5 nm and 2.3 cm^{-1} (boxcar 2.2, Gaussian 0.7) at 568.2 nm (for a Stokes shift of 1000 cm^{-1}). The frequency calibration was again performed using the 656 cm^{-1} solvent line from CS_2.

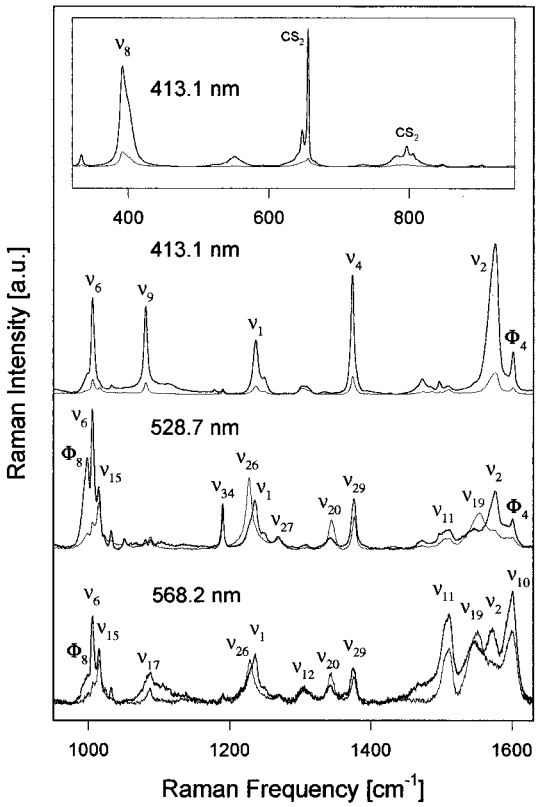

Figure 2. RR spectra of NiTPP in CS_2 measured with the indicated excitation wavelengths. The thick lines and the thin lines show the spectra measured in polarization parallel and perpendicular to the laser polarization, respectively. Typical conditions: 50 mW, 1.0 mM, spectral slit widths are below 3 cm^{-1}.

Curve Fitting. The spectra were decomposed using a novel line shape analysis program called MULTIFIT.[23] The Raman bands were fitted with a convolution of a line profile (Lorentzian or Voigtian) and the slit functions mentioned above. The spectra at different excitation wavelengths were consistently analyzed. In other words, the observed spectra were subjected to a global fit in which each Raman band has identical half-width and frequency position at all excitation wavelengths. Therefore, we can eliminate ambiguities in the band shape analysis. The spectral width and the Raman bandwidth are defined by the full width at half-maximum (fwhm), and the Raman half-widths given in the text are true widths corrected for the spectrometer slit function. Finally, a linear function (or in some cases a second-order polynomial) was employed to fit the background intensity.

3. Results

Raman Spectra. Figure 2 displays an overview of the polarized Raman spectra of NiTPP in CS_2 measured with excitation wavelengths in the B_0, Q_v, and Q_0 band. The most prominent Raman bands are labeled, thereby employing the results of a recent normal mode analysis[24] of NiTPP. In the two upper spectra measured with 413.1 nm (B band excitation), all intense Raman bands are polarized. They can therefore be attributed to A_{1g}-type vibrations (ν_8, ν_6, ν_9, ν_1, ν_4, ν_2, Φ_4). Their intensities result from Franck−Condon coupling within the strongly dipole-allowed B states.[1,22] Apparently, the depolarized bands are less intense because their intensities arise from the weaker intrastate Jahn−Teller coupling. With Q_v excitation (528.7 nm), the depolarized B_{2g} bands and the inversely polarized A_{2g} bands (to a minor extent also the depolarized B_{1g} bands) exhibit intensities comparable to those of the A_{1g} bands,

whereas the depolarized B_{1g} bands ν_{11} and ν_{10} are most intense with Q_0 excitation (568.2 nm). In the Q_0 and Q_ν band region, the intensities of the observed Raman bands result predominantly from interstate Herzberg−Teller coupling. The particularly strong intensities of B_{1g} bands observed with Q_0 excitation are likely caused by pseudo-Jahn−Teller coupling between the porphyrin ground state and an excited state constituted by an electron transfer from the d_π (Ni(II)) to the e_g orbital of the porphyrin macrocycle.[22]

Most of the Raman bands in the above spectra exhibit Lorentzian shapes. However, we have also observed several bands with asymmetric shapes, namely ν_8, Φ_8, ν_1, ν_{11}, ν_{19}, ν_2, and ν_{10}, the peak frequencies of which appear at 392, 996, 1236, 1508, 1550, 1573, and 1599 cm^{-1}, respectively. These bands are much broader than the remaining Raman lines. As it will be shown below, their band shapes depend on the excitation wavelengths. This indicates that each of these bands is composed of at least two sub-bands with different REPs.

Spectral Analysis. We have decomposed four spectral regions of the Raman spectra, the region of the band ν_8, the region around the line ν_6 (970−1050 cm^{-1}), the overlapping bands ν_1 and ν_{26}, and the fingerprint region (1450−1630 cm^{-1}). The latter is mostly crowded and contains the line Φ_4 and the core size marker bands ν_3, ν_{11}, ν_{19}, ν_2, and ν_{10}. Five bands can be resolved between 970 and 1050 cm^{-1}, Φ_8, ν_6, ν_{15}, ν_{22}, and Φ_7. All these spectral regions were subjected to the curve-fitting procedure. To account for the bands with asymmetric shapes, we assumed that these are composed of two Voigtian sub-bands. The frequency positions and half-widths of these sub-bands and also those of the bands with symmetric shapes were determined to yield the best fit to the spectra for all excitation wavelengths employed.

ν_6 Region. While the fitting parameters of isolated Raman bands (e.g. ν_8) can be easily obtained, the spectral analysis is much more complicated for the overcrowded fingerprint region between 1450 and 1630 cm^{-1} and also for the ν_6 region (970−1050 cm^{-1}). To obtain an unambiguous set of parameters, we exploited the different enhancement patterns and polarization properties of the Raman bands. This is illustrated in Figure 3. At 406.7 nm excitation, the line ν_6 dominates this B-band-type spectrum, and the correct spectral parameters can easily be obtained, namely, the band shape (Lorentzian or Voigtians), frequency, and half-width. These parameters were then fixed in the fits to the spectra measured at other wavelengths. On the contrary, the parameters of Φ_8 can most accurately be evaluated from the spectra taken with Q_ν excitation (514.5 and 528.7 nm). Once the frequency positions and the half-widths of every single Raman band in this spectral region are determined, the spectra were fitted with the whole parameter set to check whether the fits are satisfactory for all excitation wavelengths.

The parameters of the Raman bands investigated are listed in Table 1. Some of our assignments deviate from those proposed by Li et al.[24] In their study, the band at 997 cm^{-1} is assigned to the B_{2g} mode ν_{30}. We found, however, that the depolarization ratios (DPRs) of both sub-bands are about 0.125 and constant for all wavelenghts investigated, a value typical for A_{1g}-type modes. We therefore assign this band to the A_{1g}-type phenyl vibration Φ_8, the frequency position of which was calculated[24] to 1003 cm^{-1}. Moreover, Li et al. assigned the line at 1015 cm^{-1} to the A_{2g} mode ν_{22}. This is inconsistent with its DPR, which is 0.75 ± 0.3 at all excitation wavelengths. The DPR indicates a B_{1g}- or B_{2g}-type vibration. Since the line is comparatively intense with Q_0 excitation, B_{1g} is the more appropriate choice. We therefore attribute it to the mode ν_{15}.

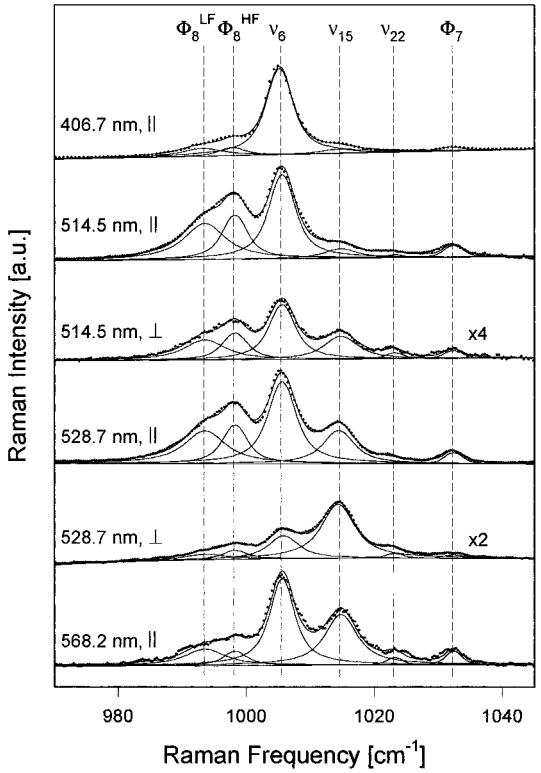

Figure 3. Decomposition of the Raman spectra in the region between 970 and 1050 cm^{-1} for different excitation wavelengths. Symbols || and ⊥ denote the parallel and perpendicular polarization. Some ⊥-spectra are scaled by a factor as indicated. Spectral slit widths are 2.8, 2.9, 2.6, and 2.2 cm^{-1} for 406.7, 514.5, 528.7, and 568.2 nm, respectively.

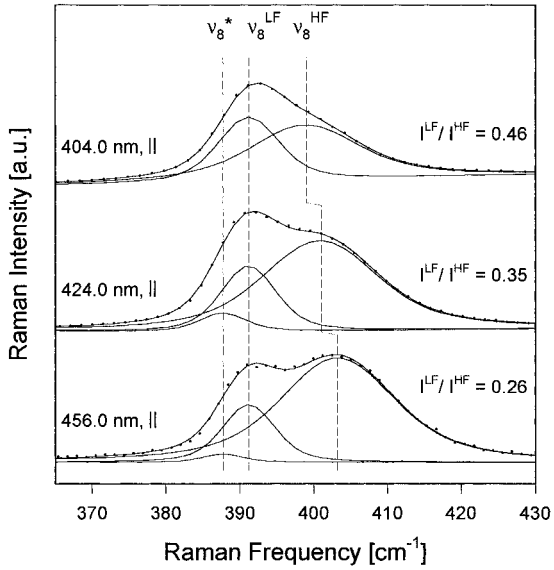

Figure 4. Decomposition of the ν_8 band measured with different excitation wavelengths and in parallel polarization. Spectral slit widths are 6.3, 5.6, and 4.5 cm^{-1} for 404, 424, and 456 nm, respectively.

The line at 1023 cm^{-1}, which Li et al. assigned to the E_u mode ν_{47}, is likely to arise from the A_{2g}-type mode ν_{22}, because its DPR is larger than 1.0.

ν_8 Region. The band ν_8 appears isolated in the spectra, so that it can conveniently be analyzed. Its band shape is clearly asymmetric (Figure 4) and can be reproduced by two sub-bands, i.e. a comparatively narrow low-frequency (LF) and a much broader high-frequency (HF) sub-band. Additionally, we observed a third line close to the LF sub-band designated as ν_8*. This line only appears in spectra measured with pulsed

TABLE 1: Spectral Parameters Derived from the Consistent Analysis of the Raman Bands: G and L Denote the Gaussian and Lorentzian Contributions to the True Raman Band Profiles (Corrected for the Spectrometer Function); The Half-Widths Γ_L, Γ_G Are Full Widths at Half-Maximum

mode	type	ν	Γ_L	Γ_G
ν_8*	A_{1g}	387.5	4.0	
ν_8^{LF}	A_{1g}	390.9	3.5	4.2
ν_8^{HF}	A_{1g}	401.0	10.3	10.4
Φ_8^{LF}	A_{1g}	993.4	7.2	
Φ_8^{HF}	A_{1g}	998.0	3.7	
ν_6	A_{1g}	1005.4	4.0	
ν_{15}	B_{1g}	1014.6	5.5	
ν_{22}?	A_{2g}?	1023.0	2.0	
Φ_7	A_{1g}	1032.2	2.0	
ν_{26}	A_{2g}	1227.4	8.7	
ν_1^{LF}	A_{1g}	1236.0	8.0	
ν_1^{HF}	A_{1g}	1248.8	8.3	
ν_3^{LF}	A_{1g}	1472.8	13.3	
ν_3^{HF}	A_{1g}	1486.1	6.5	
Φ_5	A_{1g}	1497.2	3.9	
ν_{11}^{LF}	B_{1g}	1505.6	10.2	8.0
ν_{11}^{HF}	B_{1g}	1511.9	2.0	8.6
?	A_{1g}	1529.0	8.0	14.8
ν_{19}^{LF}	A_{2g}	1546.8	9.1	15.9
ν_2*	A_{1g}	1554.0	9.0	
ν_{19}^{HF}	A_{2g}	1556.5	7.3	9.9
ν_2^{LF}	A_{1g}	1570.6	14.8	
ν_2^{HF}	A_{1g}	1577.3	2.3	6.1
?	B_{1g}, B_{2g}	1578.7	7.0	18.0
ν_{10}^{LF}	B_{1g}	1597.9	3.6	14.6
ϕ_4	A_{1g}	1601.2	4.4	
ν_{10}^{HF}	B_{1g}	1604.1	16.6	

laser excitation in the wavelength region between 390 and 460 nm, but is absent in all spectra measured with CW excitation. It is therefore attributed to porphyrin molecules in a photoexcited Ni(II) state populated by optical pumping via the B and the Q state.[25,26] To check this assignment, we have measured several spectra with different laser power (i.e. $(0.2-1.0) \times 10^8$ W/cm^2) at a single wavelength and found its intensity to significantly increase with higher laser power relative to the LF and HF sub-bands. The intensity ratio of these two sub-bands does not depend on the laser power.

We found Voigtian band shapes for both sub-bands of ν_8. This is in contradiction to the results of Jentzen et al.,[18] who fitted each sub-band with a Lorentzian. We have also performed a fit with two Lorentzians (plus a Lorentzian for ν_8*), but this did not yield a satisfactory reproduction of the band shape. We feel that the Lorentzian fit worked well in the investigation of Jentzen et al., because their analysis is based on only two Raman spectra observed at 413.1 and 457.9 nm. Our analysis, however, involves fits to a large number of spectra with a consistent parameter set. In the case of ν_8, successful fitting unambiguously requires the use of Voigtian sub-bands.

As shown in Figure 4, the intensity ratio of the ν_8 sub-bands depends strongly on the excitation wavelength. While the intensity of the LF sub-band is not much lower than that of its HF counterpart on the blue side of the B band (404 nm), the HF sub-band accounts for 79% of the bands total intensity when the exciting radiation is tuned to the low-energy side of the B band (456 nm). This is in accordance with the results of Jentzen et al., who found a comparatively more intense HF sub-band at 457.9 nm.

It should be further noted that the above two-band model (or three-band for spectra measured with pulsed excitation) does still not allow a consistent fitting of ν_8, because the frequency

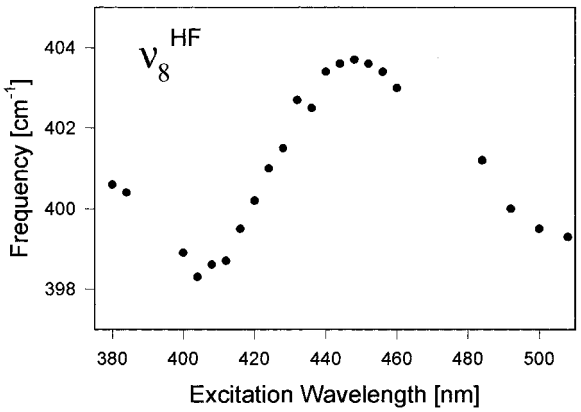

Figure 5. Peak frequency of the HF sub-band of ν_8 as a function of the excitation wavelength.

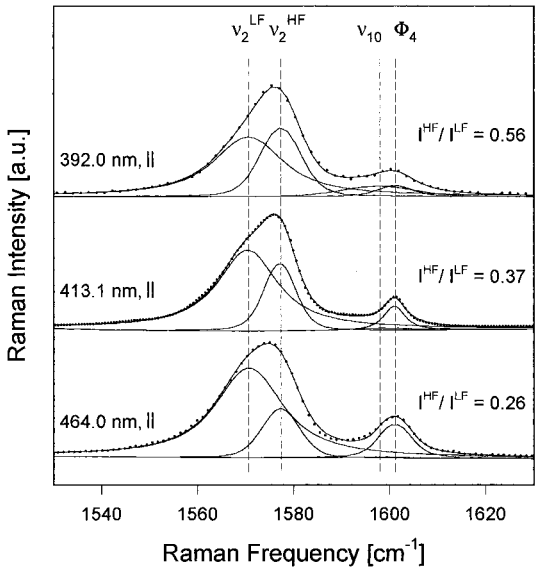

Figure 6. Decomposition of the ν_2 band measured with different excitation wavelengths and in parallel polarization. Spectral slit widths are 6.1, 2.6, and 7.0 cm^{-1} for 392, 413.1, and 464 nm, respectively.

position of the HF sub-band still slightly varies with the excitation wavelength (Figure 5). The frequency has a minimum value of 398 cm^{-1} on the blue side and a maximum value of 404 cm^{-1} on the red side of the B band resonance. As it will be shown in the discussion section, this indicates an additional conformational heterogeneity of the NiTPP ensemble in the sample.

Fingerprint Region. The fingerprint region is even more complex than the spectra between 970 and 1050 cm^{-1}. Figure 6 shows the decomposition of the spectra in preresonant and resonant B band excitation. With this excitation, the bands ν_2 and Φ_4 dominate the spectra. All other bands are weak or negligible. Therefore, the spectral parameters of ν_2 and Φ_4 can conveniently be determined. The band shape of ν_2 can well be described by two sub-bands, the intensity ratio of which depends on the excitation wavelength. Contrary to ν_8, the LF sub-band appears broad and its relative intensity increases with longer wavelengths. The intensity ratio I^{HF}/I^{LF} for this Raman band is comparable with the reciprocal value I^{LF}/I^{HF} for ν_8. This is in good accordance with the results of Jentzen et al.,[18] who found a similar behavior for the temperature dependence of ν_2 and ν_8; that is, the LF sub-band of ν_2 and the HF sub-band of ν_8 increase with decreasing temperature. These results provide strong evidence that the LF sub-band of ν_2 corresponds to the HF sub-band of ν_8 and vice versa.

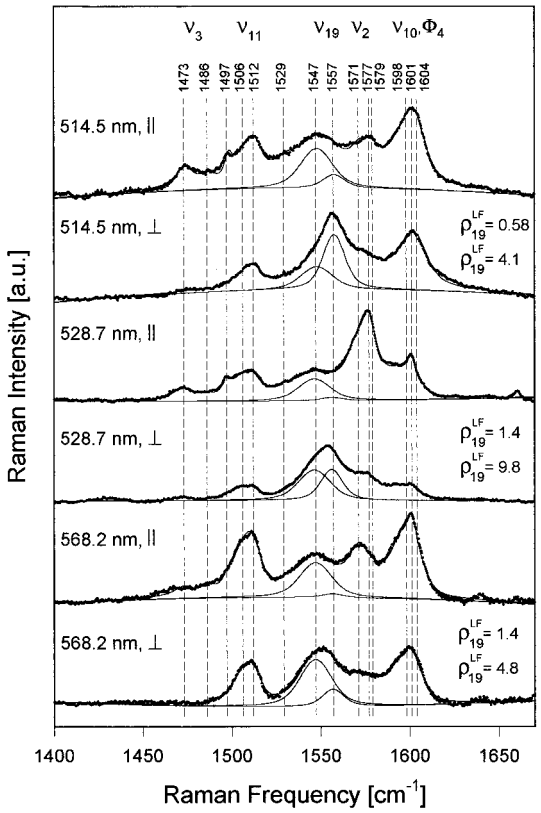

Figure 7. Decomposition of the spectra in the fingerprint region measured in Q_0 and Q_ν excitation. Symbols || and ⊥ denote the parallel and perpendicular polarization. The solid line reproducing the data is a fit calculated for all Raman bands in the spectral region. The other solid lines show the fits to the sub-bands of ν_{19}. The corresponding DPRs are listed. Spectral slit widths are 2.7, 2.5, and 2.1 cm^{-1} for 514.5, 528.7, and 568.2 nm, respectively.

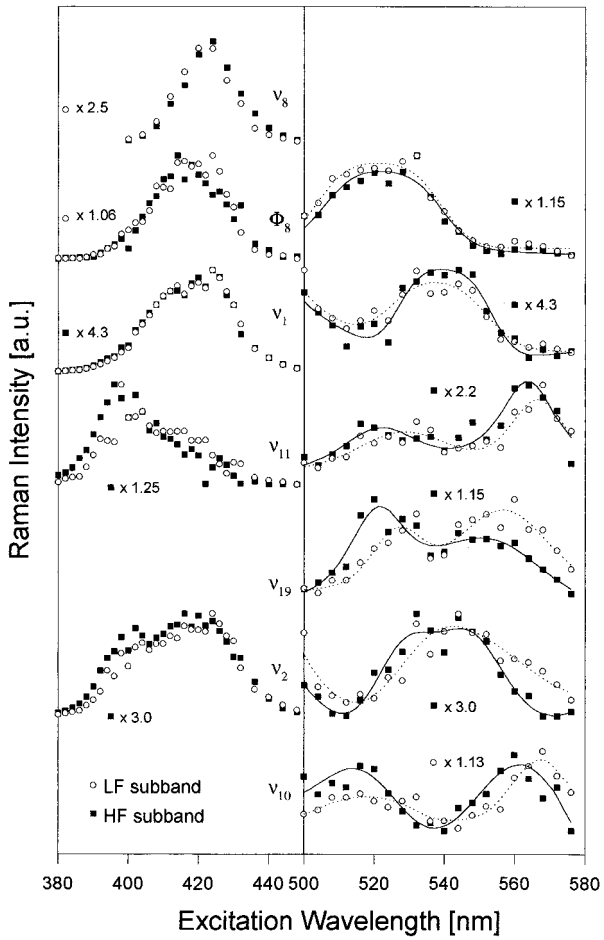

Figure 8. REPs of the sub-bands of heterogeneous Raman bands. The REPs of the smaller sub-bands are scaled onto the REP of the counterparts by the factor indicated.

The obtained band parameters for ν_2 are listed in Table 1. We again observed an additional line with pulsed excitation designated as ν_2*, which results from molecules with a photoexcited nickel state. This line does not appear in the spectra of Figures 6 and 7, because its intensity is only detectable with excimer excitation in the wavelength range between 400 and 450 nm (data not shown).

The spectra in the fingerprint region are more crowded with Q_0 and Q_ν excitation. The decomposition is depicted in Figure 7. There are some Raman bands that are not relevant for the context of this paper but which must be accounted for in the fitting procedure. The bands at 1473 and 1486 cm^{-1} are polarized and are most likely sub-bands of the band ν_3. The band ν_{11} is overlapped by a polarized line of very small halfwidth at 1497 cm^{-1}. The latter must probably be assigned to the phenyl substituent mode Φ_5. The band at 1529 cm^{-1} is also polarized and may be attributed to a combinational overtone $\nu_{12}(B_{1g}) + \nu_{13}(B_{1g})$. ν_2 is overlapped by a depolarized band at 1579 cm^{-1} that may be attributed to the overtone $\nu_8(A_{1g}) + \nu_{34}(B_{2g})$.

The large number of bands renders the analysis more difficult. However, by an appropriate selection of excitation wavelengths used for the determination of the spectral parameters the latter can be obtained with sufficient accuracy. The choice of fitting parameters is of course not unique, but this did not yield serious uncertainties in the determination of the REPs. The band parameters of ν_{11} and ν_{10} were obtained from the spectra taken with Q_0 excitation. Φ_4 overlaps with ν_{10}, but these two bands can well be separated by the fits because their halfwidths are quite different. The line at 1497 cm^{-1} does not impair the decomposition of ν_{11} due to its very low intensity and narrow bandwidth. The spectral parameters of ν_{19} were more difficult to determine owing to its overlap with two polarized bands, ν_2 and the band at 1529 cm^{-1}. It is possible, however, to eliminate the latter bands from the spectrum by subtracting the ||-spectrum multiplied by their DPR value (which is 0.125 or a slightly higher value) from the corresponding ⊥-spectrum. In the thus obtained difference spectrum the band ν_{19} appears nearly isolated, so that it can be easily decomposed. This procedure was also employed to facilitate the analysis of ν_{10}.

Resonance Excitation Profiles. We determined the REPs of the sub-bands of all heterogeneous bands investigated for excitation wavelengths between 380 and 570 nm. The results are depicted in Figure 8. The REPs of the LF sub-bands of the core size marker bands ν_{11}, ν_{19}, and ν_{10} are clearly red shifted with respect to the profiles of their HF counterparts. In order to obtain the magnitudes of the shifts, the corresponding excitation profiles were shifted against each other on a wavenumber scale to bring them to optimal coincidence. This procedure was carried out for the B as well as for the Q_0 and Q_ν resonances. Thus we obtained shifts of 160 ± 30 cm^{-1} for all REPs.

As shown in Figure 8, such a shift is less apparent for ν_8 and ν_2. However, an accurate determination of the shift is possible by comparing the intensity ratio of corresponding sub-bands with that calculated for a given shift. The result is shown in Figure 9. The solid lines therein were obtained by means of the following procedure. First we employed a single Voigtian to fit the B_0 and B_ν resonance profiles of ν_8 and two Voigtians for the corresponding resonances of ν_2. Then we shifted the fit curve by the parameter indicated in Figure 9 and divided it

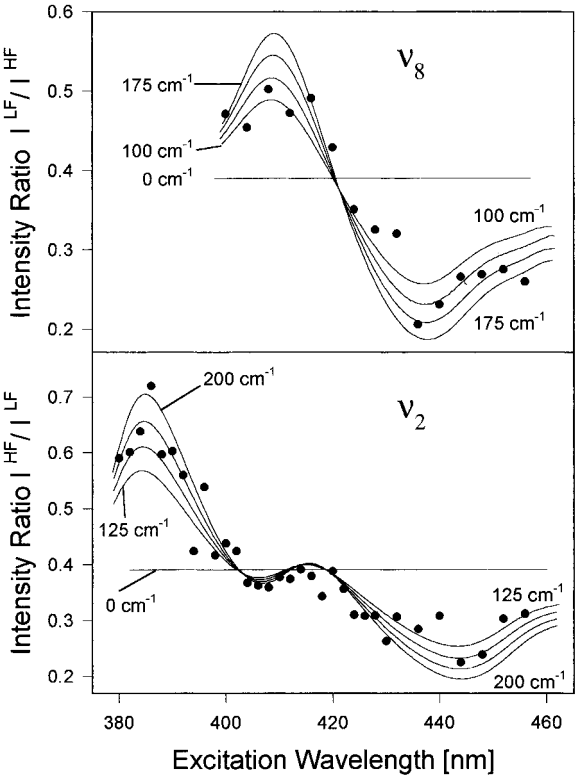

Figure 9. Intensity ratio dispersion of the sub-bands of ν_8 and ν_2. The solid lines result from a calculation explained in the text. The curve parameters give the shifts of the REPs of corresponding sub-bands with respect to each other. The curves are separated by 25 cm^{-1}.

by the nonshifted fit curve. To determine the shift, the result is compared with the experimentally obtained sub-band intensity ratio. For ν_8 the shift lies between 150 and 175 cm^{-1}, and for ν_2 between 175 and 200 cm^{-1}.

ν_2 behaves similarly to the other core size marker bands in that the REP of the LF sub-band is red shifted with respect to the profile of its HF counterpart, whereas the REP of the HF sub-band is red shifted for ν_8. Therefore, ν_8 seems to behave like an "inverse core size marker" for NiTPP.

In contrast the sub-bands of Φ_8 and ν_1 have REPs with coinciding resonance positions (see Figure 8). This suggests that the heterogeneity of these bands is of different origin than that of the core size marker bands. This will be dealt with in more detail in the Discussion section.

Depolarization Ratios. In the case of D_{4h} symmetry, the depolarization ratios (DPRs) of all Raman lines are independent of the excitation wavelength. The DPR values in this symmetry are $\rho = 0.125$ for the A_{1g} modes, $\rho = 0.75$ for the B_{1g} and the B_{2g} modes, and $\rho = \infty$ for the A_{2g} modes.[27] The measured values may slightly deviate from these theoretical values because scattered light that does not propagate along the optical axis is also collected yielding a mixture of polarizations due to parallelization at the surface of the collimator.[28] From earlier investigations[22,29] we know that the observed DPR values for D_{4h} symmetry are $\rho^{obs} \approx 30$ and $\rho^{obs} \approx 0.13$ for A_{2g} modes and A_{1g} modes, respectively.

For NiTPP, however, we observed a significant DPR dispersion in particular for the A_{2g} bands. The DPR values of ν_{26}, ν_{20}, and ν_{19} are much smaller than 30. Even looking at the spectra in Figure 2 shows that the DPR value of the band ν_{20} is about 3 at 528.7 nm and 2 at 568.2 nm. Moreover, the line ν_{26} exhibits significant intensity not only in the ⊥-spectrum but also in the ||-spectrum. This is illustrated in Figure 10. Herein, ν_{26} appears as a shoulder in the ||-spectrum. It can be ruled out

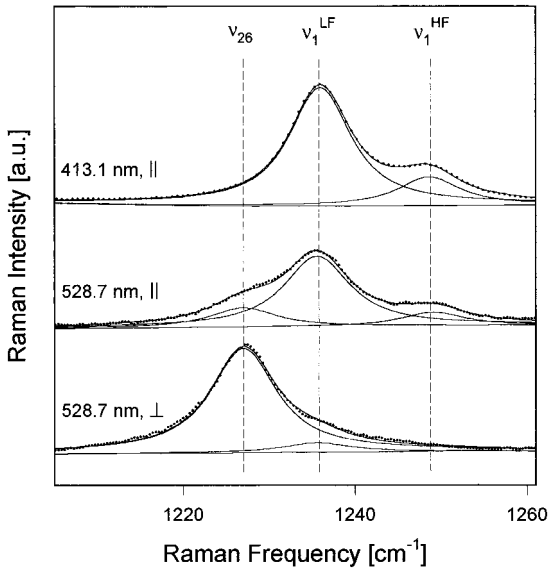

Figure 10. Decomposition of the overlapping ν_1 and ν_{26} band for different excitation wavelengths. Symbols || and ⊥ denote the parallel and perpendicular polarization. Spectral slit widths are 2.7 and 2.6 cm^{-1} for 413.1 and 528.7 nm, respectively.

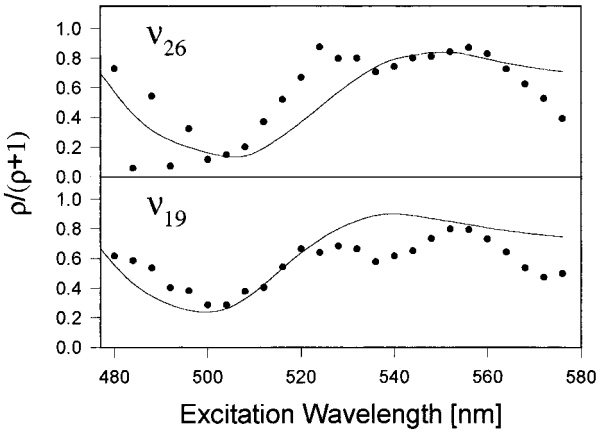

Figure 11. DPDs of the A_{2g} lines ν_{26} and ν_{19}. The solid lines result from fits that are explained in the text.

that this shoulder is a sub-band of ν_1 because it does not appear in the spectra measured with B band excitation.

As shown in Figure 7, the band ν_{19} also has significant intensity in the ||-spectra. In view of the complexity of the fingerprint region, one may suspect that the spectra are crowded by nonresolved Raman bands. However, no additional band is theoretically expected to appear near the frequeny position of ν_{19}. Therefore it is very likely that the lowering of its DPR is significant. A similar argumentation also applies for ν_{26} and ν_{20}. Li[30] has measured the polarized Raman spectra of NiTPP substituted with different isotopes in CS_2 solution. At 530.9 nm, ν_{20} displays a significant intensity in the ||-spectra of all species (Figure 3 of ref 30). Because the Raman bands exhibit different isotopic shifts, it is very unlikely that another band is responsible for the deviation of the DPR from its D_{4h} value. For the line ν_{26} the spectra of the ^{15}N and d_{20} isotopomers are especially interesting, because the line ν_{26} is herein separated from ν_1. The spectra clearly show that the DPR of ν_{26} is not significantly larger than 2.

The DPDs of ν_{26} and ν_{19} are depicted in Figure 11. Although we have measured the DPDs in a much larger wavelength interval (from 380 to 576 nm), only the region of the Q_ν and Q_0 resonance is shown, because the A_{2g} bands are very weak outside these resonances, and the DPR can therefore not

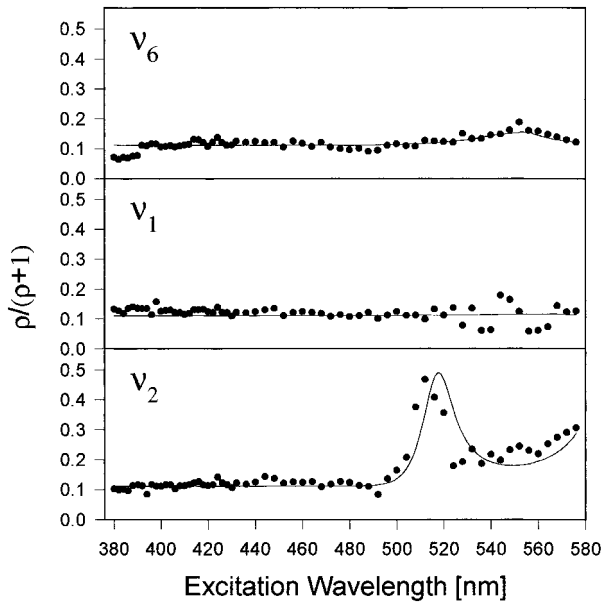

Figure 12. DPDs of the A_{1g} lines ν_6, ν_1, and ν_2. The solid lines result from fits that are explained in the text.

accurately be determined. The solid lines are calculated with the theoretical approach[22] previously used for nickel(II) porphine (NiP) including multimode contributions of 15 Raman-active fundamental modes.[29] To account for symmetry-lowering distortions of the porphyrin macrocycle, an electronic perturbation $\delta a_{2g} = 150$ cm^{-1} of symmetry type A_{2g}, which mixes the electronic wave functions, was introduced into the time independent perturbation expansion of the vibronic wave functions. As can be seen in Figure 11, the calculated dispersion curves give a coarse reproduction of the data.

Bands resulting from modes of symmetry types other than A_{2g} show no or only a weak dispersion. The DPDs of the polarized bands with the largest Raman intensities in Q_ν and Q_0 resonance are shown in Figure 12. Only the ν_2 shows a significant dispersion. It is interesting to note in this context that these weak dispersions are very well reproduced by the calculations with the same value of δa_{2g}. We therefore conclude that the effect of the macrocycle distortions on the DPDs of NiTPP can be satisfactorily described by taking into account only the perturbation of the electronic wave functions.

Other A_{1g} lines such as Φ_8, ν_9, ν_4, and Φ_4 show only weak or negligible DPR dispersions (data shown in ref 29). As theoretically expected, all depolarized bands investigated (ν_{15}, ν_{11}, ν_{10}, ν_{34}, ν_{27}, and ν_{29}) show no significant DPR dispersion (data shown in ref 29).

It must be emphasized that all DPDs shown above are determined by the whole band intensities. In other words, we have not distinguished between different sub-bands. However, a DPR dispersion is only expected for the sub-bands attributed to the nonplanar conformer. We will refer to this point in the Discussion section.

4. Discussion

Conformers. Our analysis of the band shapes of the structurally sensitive Raman bands ν_8, ν_{11}, ν_{19}, ν_2, and ν_{10} shows that each of these bands is composed of two sub-bands with different widths. Their intensity ratio and as a consequence also the total band shape depend on the excitation wavelength. The REPs of the ν_8 mode's HF sub-band as well as those of the core size marker modes' ν_{11}, ν_{19}, ν_2, and ν_{10} LF sub-bands are red shifted with respect to the excitation profiles of their counterparts. Since the UV−visible absorption bands are shifted to lower wavenumbers by nonplanar distortions,[13] the sub-bands with red-shifted profiles are attributed to a nonplanar conformer. The other sub-bands correspond to a planar or a quasiplanar conformer. Therefore, our analysis confirms that two conformers of NiTPP coexist in CS_2 solution.[18]

The sub-bands arising from the nonplanar conformer are much broader than the corresponding sub-bands of the planar one. Only the band ν_{10} is underlied by two sub-bands with comparable widths. However, because of the high spectral crowding in the wavenumber region of this band, its fitting parameters cannot be determined as unambiguously as those for the other heterogeneous bands. Therefore, we cannot exclude that also in this case the LF sub-band is broader than the HF sub-band. As can be seen from Table 1, the large width of the LF sub-bands of ν_2 and ν_{11} mainly results from the Lorentzian contributions. Therefore, it is likely that these large widths can be explained by a more rapid vibrational dephasing[31] in the nonplanar conformation compared to the planar one. The Gaussian contributions of the LF sub-bands of ν_{19} and ν_{10} seem to indicate an additional broadening mechanism. However, the band shapes of these sub-bands are determined less accurately because of the strong spectral overlap. Therefore it cannot be ruled out that they are also pure Lorentzians.

The HF sub-band of ν_8, however, exhibits a significant Gaussian contribution. This indicates an additional heterogeneity for the nonplanar species. This heterogeneity is due either to a finite number of subconformers or to a continuous (e.g. Gaussian) distribution of slightly different subconformations. If the frequency position of ν_8 is slightly different for the subconformers, the band shape of this sub-band can be understood as a superposition of Lorentzians, where each Lorentzian belongs to one subconformer.

The assumption of two different subconformers gives also a reasonable explanation for the shift of the sub-band ν_8^{HF}. This can easily be understood, if one assumes two subconformers with REPs shifted with respect to each other. If the REP of the subconformer with higher Raman frequency is red shifted, the respective subsub-band is more enhanced on the red side of the Soret band, causing an upshift of the total sub-band. On the blue side, however, the low-frequency part of this sub-band is more enhanced, leading to a downshift of ν_8^{HF}. This can explain the wavelength dependence of the position of ν_8^{HF} shown in Figure 5. Obviously, other bands are less sensitive to the conformational difference of the subconformations, because the respective sub-bands exhibit no significant shift. It is therefore reasonable that these sub-bands have only small Gaussian contributions. The situation is different for NiOEP, where the LF sub-bands of ν_{19} and ν_{10} have large Gaussian contributions.[17] This suggests that the subconformational heterogeneity is distributed along different coordinates for these two porphyrins.

It is noteworthy that the above results parallel findings from previous investigations[16,17] on NiOEP in CS_2, which also have revealed the coexistence of planar and nonplanar conformers. The sub-bands resulting from the nonplanar conformer of NiOEP appear also on the low-frequency side of the core size marker bands, and their REPs are also red shifted.

The REPs of the sub-bands of ν_1 and Φ_8 are not shifted with respect to each other. Therefore, the sub-bands cannot arise from planar and nonplanar conformations. According to the potential energy distribution reported by Li et al.,[24] these bands arise from modes with large contributions from the C_m-C_{phenyl} stretching motions. Thus, it is reasonable to assign the above sub-bands to additional conformations with different orientations of the phenyl substituents. Similarly different conformers were

previously found[16,29] for NiOEP in CS_2. Its ν_8 consists of two sub-bands, which were suggested to correspond to conformers with different orientations of the ethyl substituents.[24] Confirming this interpretation, we have evidence that the REPs of the ν_8 sub-bands in NiOEP are not shifted with respect to each other, and therefore these sub-bands cannot arise from planar and nonplanar species. Thus, NiOEP coexists in more than two conformations. Analogously it is conceivable that NiTPP also has additional species.

However, there is some evidence against the existence of different rotational isomeres of the phenyl substituents. The HF sub-band of the ν_1 mode is also present in the spectra of a NiTPP single crystal.[18] Because the crystal contains only one conformation, the appearence of the HF-sub-band would contradict the above model. Therefore, it is more likely that the ν_1 doublet is caused by Fermi resonance with the overtone $\nu_{13} + \nu_{15}$. Fermi resonance has also been suggested to explain the asymmetric bands or doublets found for NiP, CuP, and CoP.[32] However, no combination of fundamentals could be found to explain the asymmetry of the band Φ_8. Therefore, a final interpretation for its doublet cannot be given.

Distortion of the Porphyrin Macrocycle. The dispersion of the DPRs shows that symmetry-lowering perturbations are operative, which reduce the porphyrins' ideal D_{4h} symmetry. In general there are two possible origins for such perturbations.[1] First, substituents may have an influence on the electronic structure of the macrocycle, and an asymmetric arrangement of them can therefore lower the symmetry of the electronic wavefunctions. Second, noncovalent interactions between substituents as well as between substituents and adjacent pyrrole rings may cause nonplanar distortions. Third, the macrocycle may be distorted from the ideal D_{4h} symmetry by a central ion with a small radius as it is probably the case for nickel(II) in NiOEP.[11,17] In view of the symmetric arrangement of the phenyl substituents, planar deviations from D_{4h} are unlikely. Therefore, the DPR dispersion suggests a nonplanar conformation. However, previous investigations[20] have shown that no dispersion is caused if only one type of out-of-plane distortion (e.g. B_{1u}) is effective. Thus, at least two distortions of different symmetry must be invoked to explain our data.

As mentioned above, crystallized NiTPP exhibits a nonplanar macrocycle.[18] In order to determine the symmetry types and the magnitude of the distortions, Jentzen et al.[5] applied a recently developed structural decomposition method. These authors have shown that an appropriate reproduction of the structures of various synthetic porphyrins and heme groups in protein matrices emerging from crystallographic studies solely requires considering distortions along the normal coordinates of the lowest frequency modes. These are the A_{2u} mode γ_9 (doming), the B_{1u} mode γ_{14} (ruffling), and the B_{2u} mode γ_{18} (saddling). For the NiTPP crystallographic structure the decomposition method[18] reveals strong ruffling with a total distortion[33] of 1.296 Å and moderate saddling with a total distortion of 0.027 Å.

If one assumes that the nonplanar conformation of NiTPP in solution is identical with that in the crystal, it is possible to calculate the perturbation term corresponding to the B_{1u} and B_{2u} distortions. The electronic perturbation Hamiltonian $\hat{H}'$ in terms of the mass-weighted normal distortions $\delta\bar{Q}_{B1u}$ and $\delta\bar{Q}_{B2u}$ is given by[1]

$$\hat{H}' = \frac{\partial^2 \hat{H}}{\partial Q_{B1u}\, \partial Q_{B2u}} \delta\bar{Q}_{B1u}\, \delta\bar{Q}_{B2u} \tag{1}$$

where $\hat{H}$ is the electronic Hamiltonian of the D_{4h} symmetric undistorted macrocycle. $\hat{H}'$ describes a perturbation of symmetry type A_{2g}, because $\Gamma_{B1u} \times \Gamma_{B2u} = \Gamma_{A2g}$.

$\delta\bar{Q}_{B1u}$ can be calculated by virtue of[34]

$$\delta\bar{Q}_{B1u} = \delta\bar{Q}_{\gamma 14} = \sqrt{\sum_i m_i \Delta_i^2(\gamma_{14})} \tag{2}$$

where $\Delta_i(\gamma_{14})$ are the Cartesian displacements of the ith atom corresponding to the distortion along the normal coordinate γ_{14} and m_i is the atomic mass. Inserting the $\Delta_i(\gamma_{14})$ values derived from the above decomposition method into eq 2 reveals $\delta\bar{Q}_{B2u} = 1.9 \times 10^{-23}$ m $\sqrt{\text{kg}}$. Similarly the distortion along the coordinate γ_{18} is calculated as $\delta\bar{Q}_{B2u} = 0.34 \times 10^{-23}$ m $\sqrt{\text{kg}}$. Hence, we estimate the product of these static distortions as

$$\delta\bar{Q}_{B1u}\, \delta\bar{Q}_{B2u} = 0.65 \times 10^{-46}\ \text{kg m}^2 \tag{3}$$

The second derivative of the Hamiltonian in eq 1 can be evaluated from the vibronic coupling matrix element which contributes to the intensity of the combinational overtone $\gamma_{14} + \gamma_{18}$

$$\hat{H}' = \frac{\partial^2 \hat{H}}{\partial Q_{B1u}\, \partial Q_{B2u}} Q_{B1u} Q_{B2u} \tag{4}$$

Q_{B1u} and Q_{B2u} are the vibronic matrix elements $\langle 0|Q_{B1u}|1_{B1u}\rangle$ and $\langle 0|Q_{B2u}|1_{B2u}\rangle$, which are equal to the square root of the mean quadratic elongations of the respective harmonic vibrations. The product $Q_{B1u}Q_{B2u}$ is given by

$$Q_{B1u}Q_{B2u} = \sqrt{\frac{\hbar}{4\pi c \Omega_{14}}}\sqrt{\frac{\hbar}{4\pi c \Omega_{18}}} = 0.56 \times 10^{-47}\ \text{kg m}^2 \tag{5}$$

Comparison of eq 3 and eq 5 reveals that the static perturbation in eq 1 is more than 11 times larger than the vibronic coupling in eq 4. Since we have not analyzed the excitation profile of the combinational overtone $\gamma_{14} + \gamma_{18}$, the vibronic coupling for this mode can only be roughly estimated. To this end, the intensities of the overtone bands must be compared with those of the fundamental bands. The strongest overtone bands appearing in the spectra of NiP, NiOEP, and NiTPP in the wavenumber range below 1700 cm^{-1} correspond to the combined vibrations $\nu_8 + \nu_{26}$, $\nu_7 + \nu_8$, and $\nu_8 + \nu_{24}$ of NiP. The line assigned to $\nu_8 + \nu_{26}$ at 1683 cm^{-1} is only a factor of 5 weaker than the two strongest A_{2g} lines ν_{26} and ν_{19} (data not shown). The Raman lines corresponding to $\nu_7 + \nu_8$ at 1090 cm^{-1} and $\nu_8 + \nu_{24}$ at 1180 cm^{-1} are less intense, but not much more than 10 times weaker than the strongest A_{1g} line. Other overtone bands generally exhibit much smaller intensities. These bands are weaker by at least a factor of several tens. It is therefore reasonable to assume that the vibronic coupling term in eq 4 is 1 order of magnitude smaller than the linear coupling terms, i.e.

$$\left\langle Q\left|\frac{\partial^2 \hat{H}}{\partial Q_{B1u}\, \partial Q_{B2u}}\right|B\right\rangle Q_{B1u}Q_{B2u} \approx 0.1\left\langle Q\left|\frac{\partial \hat{H}}{\partial Q_{A2g}}\right|B\right\rangle Q_{A2g} \tag{6}$$

Earlier studies[19,22] have shown that linear vibronic coupling elements are in the range of some 100 cm^{-1}. Therefore, the order of magnitude for the quadratic coupling term in eq 4 is about 10 cm^{-1}. Since the static A_{2g}-type perturbation term in eq 1 is more than 11 times larger, this is consistent with the value of 150 cm^{-1} determined by the analysis of the observed DPDs.[29]

For the planar conformer one does not expect any DPR dispersion. For heterogeneous Raman bands exhibiting a DPR dispersion, the dispersion must therefore solely arise from the sub-band of the nonplanar conformer. This can be illustrated by the A_{2g} band ν_{19} in Figure 7. In D_{4h} symmetry, its DPR is expected to be ∞, which means that the intensity is zero in parallel polarization. This is indeed approximately the case for the HF sub-band. Its intensity is not exactly zero, but it cannot be ruled out that this is caused by improper fitting to the complex spectra. The LF sub-band, however, exhibits significant intensity in the parallel spectra. The DPRs of both sub-bands are indicated in Figure 7. Compared to porphyrins with no DPR dispersion such as NiP and NiOEP, where DPR values of about $\rho \approx 30$ are observed for the A_{2g} lines,[22,29] the DPR of the LF sub-band is very low. It is therefore evident that the dispersion arises from this sub-band.

Raman Lines from the Excited Nickel(II) State. Some spectra measured with pulsed laser excitation exhibit additional Raman lines which are absent in the spectra recorded with CW excitation. Such lines were also observed for other porphyrins, e.g. nickel(II) octaethylporphyrin (NiOEP),[25,29] free base tetraphenylporphyrin (H_2TPP),[35,36] zinc(II) tetraphenylporphyrin (ZnTPP),[37] and some copper porphyrins in coordinative solvents such as CuOEP and CuTPP.[26] However, these lines are absent for CuOEP in CS_2 solution.[29]

The additional Raman lines result from excited states of the porphyrin, which are populated by optical pumping via the two lowest excited singlet states of the macrocycle Q and B into a metastable state with lower energy. The relaxation processes have been extensively studied by picosecond transient absorption spectroscopy.[38−40] The photoexcitation is followed by an extremely fast intersystem crossing ($\tau < 1$ ps) into the triplet T_1 state (π,π^*), which has the same electronic configuration as the Q state. For porphyrins with central d-shell transition metal ions such as Ni(II) or Cu(II), the molecule can relax from the T_1 state to the first excited (d,d) state of the central ion. The (d,d) state has a lifetime large enough to get significantly populated. Therefore, Raman scattering occurs not only from the ground state but also from the the (d,d) state. The latter is responsible for the additional Raman lines observed for NiOEP and NiTPP.[41]

It is noteworthy in this context that for copper porphyrins such lines are only observed in coordinative solvents.[26] At our experimental conditions, however, no additional lines appear in the spectra with pulsed excitation (data not shown). This can be explained by the long lifetime of the state T_1 ($\tau \approx 120$ ns), which is 3 orders of magnitude higher than for nickel porphyrins ($\tau \approx 290$ ps)[26] or for copper porphyrins in coordinative solvents, where τ is on the order of 100 ps. In pump and probe experiments additional Raman lines were also observed for copper porphyrins in noncoordinative solvents,[42] but these lines are attributed to the state T_1. Such triplet Raman spectra were also obtained for free base and zinc porphyrins.[35,36] These results confirm that the additional Raman lines are a consequence of the population of an excited (d,d) state of the central ion.

Because of the large dipole transition moment of the B band, the Raman lines from excited states exhibit comparably large intensity with B band excitation. If the excitation wavelength is varied from the B band maximum to the preresonant region, the intensity decreases much faster than that of the "normal" Raman lines and is small or negligible between B and Q_ν resonance and in the Q_0 and Q_ν region. This is the reason why ν_8* and ν_2* are weak in the spectra shown in Figures 4 and 6.

5. Summary

The existence of at least two conformations of NiTPP in CS_2 accounts for the asymmetric shapes of ν_8 and the core size marker bands. One conformer is probably planar. From the dispersions of the depolarization ratios it can be concluded that for the other conformer at least two symmetry-lowering distortions are operative, namely ruffling and saddling. The resonance excitation profiles of the sub-bands corresponding to the nonplanar conformer are red shifted by 160 ± 30 cm^{-1} with respect to their counterparts of the planar conformer. The high-frequency sub-band of ν_8 has a strong Gaussian contribution, and its frequency position depends of the excitation wavelength. This is indicative of subconformations for the nonplanar conformer.

Acknowledgment. We thank Drs.W. Jentzen, I. Turowska-Tyrk, W. R. Scheidt, and J. A. Shelnutt for providing us with unpublished results of their decomposition method carried out for NiTPP and a copy of their manuscript prior to publication. We also thank C. Lemke for helpful discussions and for reading the manuscript.

References and Notes

(1) Schweitzer-Stenner, R. *Q. Rev. Biophys.* **1989**, *22*, 381−479.
(2) Schweitzer-Stenner, R.; Dreybrodt, W. *J. Raman Spectrosc.* **1992**, *23*, 539−550.
(3) Schweitzer-Stenner, R.; Wedekind, D.; Dreybrodt, W. *Biophys. J.* **1986**, *49*, 1077−1088.
(4) Schweitzer-Stenner, R.; Bobinger, U.; Dreybrodt, W. *J. Raman Spectrosc.* **1991**, *22*, 65−78.
(5) Jentzen, W.; Song, X.-Z.; Shelnutt, J. A. *J. Phys. Chem.* **1997**, *101*, 1684−1699. (b) Jentzen, W.; Shelnutt, J. A. *Biochemistry*, submitted for publication.
(6) Deisenhofer, J.; Epp, O.; Miki, K.; Huber, R.; Michel, H. *Nature* **1985**, *318*, 618. (b) Deisenhofer, J.; Michel, H. *Angew. Chem. Int. Ed. Engl.* **1989**, *28*, 829−847. (c) Deisenhofer, J.; Michel, H. *Science* **1989**, *245*, 1463−1473.
(7) Barkigia, K. M.; Chantranupong, L.; Smith, K. M.; Fajer, J. *J. Am. Chem. Soc.* **1988**, *110*, 7566−7567.
(8) Furenlid, L. R.; Renner, M. W.; Smith, K. M.; Fajer, J. *J. Am. Chem. Soc.* **1990**, *112*, 1634−1635. (b) Furenlid, L. R.; Renner, M. W.; Smith, K. M.; Fajer, J. *J. Am. Chem. Soc.* **1990**, *112*, 8987−8989.
(9) Shelnutt, J. A.; Medforth, C. J.; Berber, M. D.; Barkigia, K. M.; Smith, K. M. *J. Am. Chem. Soc.* **1991**, *113*, 4077−4087.
(10) Prendergast, K.; Spiro, T. G. *J. Am. Chem. Soc.* **1992**, *114*, 3793−3801.
(11) Shelnutt, J. A.; Majumder, S. A.; Sparks, L. D.; Hobbs, J. D.; Medforth, C. J.; Senge, M. O.; Smith, K. M.; Miura, M.; Luo, L.; Quirke, J. M. E *J. Raman Spectrosc.* **1992**, *23*, 523−529.
(12) Hobbs, J. D.; Majumder, S. A.; Luo, L.; Sickelsmith, A.; Quirke, J. M. E; Medforth, C. J.; Smith, K. M.; Shelnutt, J. A. *J. Am. Chem. Soc.* **1994**, *116*, 3261−3270.
(13) Jentzen, W.; Simpson, M. C.; Hobbs, J. D.; Song, X.; Ema, T.; Nelson, N. Y.; Medforth, C. J.; Smith, K. M.; Veyrat, M.; Mazzanti, M.; Ramasseul, R.; Marchon, J.-C.; Takeuchi, T.; Goddard, W. A., III; Shelnutt, J. A. *J. Am. Chem. Soc.* **1995**, *117*, 11085−11097.
(14) Song, X.-Z.; Jentzen, W.; Jia, S.; Jacquinod, L.; Nurco, D. J.; Medforth, C. J.; Smith, K. M.; Shelnutt, J. A. *J. Am. Chem. Soc.* **1997**, *118* (51), 12975−12988.
(15) Meyer, E. F., Jr. *Acta Crystallogr.* **1972**, *B28*, 2162−2167. (b) Cullen, D. L.; Meyer, E. F., Jr. *J. Am. Chem. Soc.* **1974**, *96*, 2095−2102. (c) Brennan, T. D.; Scheidt, W. R.; Shelnutt, J. A. *J. Am. Chem. Soc.* **1988**, *110*, 3919−3924.
(16) Jentzen, W. Ph.D. Thesis, University of Bremen, Germany, Jan 1994.
(17) Jentzen, W.; Unger, E.; Karvounis, G.; Shelnutt, J. A.; Dreybrodt, W.; Schweitzer-Stenner, R. *J. Phys. Chem.* **1996**, *100*, 14184−14191.
(18) Jentzen, W.; Unger, E.; Song, X.; Turowska-Tyrk, I.; Schweitzer-Stenner, R.; Dreybrodt, W.; Scheidt, W. R.; Shelnutt, J. A. *J. Phys. Chem.*, in press.
(19) Schweitzer-Stenner, R.; Stichternath, A.; Dreybrodt, W.; Jentzen, W.; Song, X.; Shelnutt, J. A.; Nielsen, O. F.; Medforth, C. J.; Smith, K. M. *J. Chem. Phys.*, in press.
(20) Lemke, C.; Shelnutt, J. A.; Quirke, J. M. E.; Schweitzer-Stenner, R.; Dreybrodt, W. *Proceedings of the Fifteenth International Conference on Raman Spectroscopy*; Asher, S. A., Stein, P., Eds.; Pittsburgh, PA, 1996, p 270.

(21) Through this work we use the word "line" for simple Lorentzian peaks and "band" for peaks with a Gaussian contribution or an asymmetric shape.

(22) Unger, E.; Bobinger, U.; Dreybrodt, W.; Schweitzer-Stenner, R. *J. Phys. Chem.* **1993**, *97*, 9956−9968.

(23) Karvounis, G.; Unger, E. Manuscript in preparation.

(24) Li, X. Y.; Czernuszewicz, R. S.; Kincaid, J. R.; Su, Y. O.; Spiro, T. G. *J. Phys. Chem.* **1990**, *94*, 31−46.

(25) Courtney, S. H.; Jedju, T. M.; Friedman, J. M.; Rothberg, L.; Alden, R. G.; Park, M. S.; Ondrias, M. R. *J. Opt. Soc. Am.* **1990**, *7*, 1610−1614.

(26) Kruglik, S. G.; Apanasevich, P. A.; Chirvony, V. S.; Kvach, V. V.; Orlovich, V. A. *J. Phys. Chem.* **1995**, *99*, 2978−2995.

(27) Spiro, T. G.; Strekas, T. C. *J. Am. Chem. Soc.* **1974**, *96*, 338−345.

(28) Turell, G. In *Practical Raman Spectroscopy*; Gardiner, D. J., Graves, P. R., Eds.; Springer Verlag: Berlin, 1989.

(29) Unger, E. Ph.D. Thesis, University of Bremen, Germany, May 1996.

(30) Li, X. Y. Ph.D. Thesis, Princeton University, 1988.

(31) Harris, C. B.; Shelby, R. M.; Cornelius, P. A. *Phys. Rev. Lett.* **1977**, *24*, 1415−1418.

(32) Jentzen, W.; Turowska-Tyrk, I.; Scheidt, W. R.; Shelnutt, J. A. *Inorg. Chem.* **1996**, *35*, 3559−3567.

(33) The total distortion is defined as the square root of the sum of all squared Cartesian displacements from an ideal D_{4h} geometry.

(34) This relationship can be derived by considering the kinetic energy of one normal vibration, i.e. $(1/2)\dot{Q}^2 = (1/2)\sum_i m_i\dot{\Delta}_i^2$. Because all atomic vibrations are either in-phase or out-of-phase, Q^2 and Δ_i^2 have the same time dependence. Therefore, the square root of the integrated equation yields the above expression.

(35) de Paula, J. C.; Walters, V. A.; Nutaitis, C.; Lind, J.; Hall, K. *J. Phys. Chem.* **1992**, *96*, 10591−10594.

(36) Bell, S. E. J.; Al-Obaidi, A. H. R.; Hegarty, M. J. N.; McGarvey, J. J.; Hester, R. E. *J. Phys. Chem.* **1995**, *99*, 3959−3964.

(37) Walters, V. A.; de Paula, J. C.; Babcock, G. T.; Leroi, G. E. *J. Am. Chem. Soc.* **1989**, *111*, 8300.

(38) Dzhagarov, B. M.; Chirvony, V. S.; Gurinovich, G. P. In *Laser Picosecond Spectroscopy and Photochemistry of Biomolecules*; Letokhov, V. S., Ed.; Adam Hilger: Bristol and Philadelphia, 1987, Chapter 3.

(39) Kobayashi, T.; Huppert, D.; Straub, K. D.; Rentzepis, P. M. *J. Chem. Phys.* **1979**, *70*, 1720.

(40) Kim, D.; Holten, D.; Gouterman, M. *J. Am. Chem. Soc.* **1984**, *106*, 2793.

(41) Findsen, E. W.; Shelnutt, J. A.; Friedman, J. M.; Ondrias, M. R. *Chem. Phys. Lett.* **1986**, *126*, 465.

(42) Asano-Someda, M.; Sato, S.; Aoyage, K.; Kitagawa, T. *J. Phys. Chem.* **1995**, *99*, 13800−13807.